

Reaction-diffusion Equations: From Semigroup Theory to Pattern Formation

Diffusion-Driven Instabilities

Steffen Bauer

April 14, 2021

1 Introduction

Modeling the spread of epidemics becomes more and more important. Often very simple models, that can even provide helpful insights for understanding the evolution of the diseases, are related to ordinary differential equations. For very high numbers of individuals this is quite reasonable. But modeling human movements or even behavior makes them very complex. An interesting method of incorporating these processes into ODE models is the use of reaction diffusion equations, where the event of getting infected is interpreted as a reaction between a susceptible and an infectious individual, the movement by diffusion and the avoidance of spots with high concentrations of known infectious as cross-diffusion. We model the epidemic not on a continuous medium but on a network that resembles the structure of, e.g., cities and connections between them. The theory for diffusion-driven instabilities can be applied and patterns with infection related interpretation can be derived. First we define the differential equations that model the spread of the disease and adapt them to the network structure. Then we analyze this by means of linearization and Turing bifurcation. Finally a few examples of numerical simulations are presented and we try to interpret them.

This work is mainly based on a paper of Chang et al. [2] and the lecture on reaction-diffusion equations of Professor Dr. Anna Marciniak-Czochra and Chris Kowall in the winter term 2020/21 in Heidelberg.

2 SIR model on networks

The classic SIR model for describing epidemic diseases is the Kermack-McKendrick model [1] of three coupled nonlinear ordinary differential equations

$$\begin{aligned}\frac{dS}{dt} &= -\beta SI, \\ \frac{dI}{dt} &= \beta SI - \gamma I, \\ \frac{dR}{dt} &= \gamma I,\end{aligned}\tag{1}$$

where t is time, $S(t)$ is the concentration of susceptible, $I(t)$ of infectious and $R(t)$ of recovered and thus immune. The population is assumed constant in size and

homogeneous structured. Parameter β is the infection rate and γ is the recovery rate. To take more realistic effects into account Chang et al. modeled in [2] human movement and behavior as diffusion and cross-diffusion

$$\begin{aligned}\frac{dS}{dt} &= f(S, I) + d_{11}\Delta S + d_{12}\Delta I \\ \frac{dI}{dt} &= g(S, I) + d_{22}\Delta I \\ \frac{dR}{dt} &= \gamma I - \delta R + d_{33}\Delta R,\end{aligned}\tag{2}$$

with more nonlinear reactions terms

$$\begin{aligned}f(S, I) &= \alpha - \beta SI^2 - \delta S, \\ g(S, I) &= \beta SI^2 - (\delta + \mu + \gamma)I,\end{aligned}\tag{3}$$

where additionally α is the population's natural birth rate, δ the natural mortality rate, and μ the disease-related mortality rate. This system of reaction diffusion equations describes movements by diffusion in a two-dimensional space with Laplacian operator $\Delta = \partial^2/\partial x^2 + \partial^2/\partial y^2$ and positive parameters d_{11}, d_{22}, d_{33} . Human behavior is modeled by cross-diffusion with coefficient d_{12} , where $d_{12} > 0$ describes movement of the susceptible individuals in direction of lower concentrations of infectious (avoidance), for $d_{12} < 0$ in direction of higher concentrations. The quadratic dependency of the reaction terms on I is due to saturation or multiple exposure before getting infected. Initial conditions are $S(0) > 0$, $I(0) > 0$ and $R(0) \geq 0$ and we impose zero-flux boundary conditions

$$\left. \frac{\partial S}{\partial \nu} \right|_{\partial \Omega} = \left. \frac{\partial I}{\partial \nu} \right|_{\partial \Omega} = \left. \frac{\partial R}{\partial \nu} \right|_{\partial \Omega} = 0, \quad \Omega \subset \mathbb{R}^2.\tag{4}$$

Remark 1. Equations for S and I in (2) without cross-diffusion are in fact an autocatalytic Gray-Scott Model which indicates the richness of emerging Turing patterns.

Instead of considering the evolving disease on a continuous space, we discretize the spatial aspects on a graph, where nodes resemble, e.g., cities and edges connections like highways, rail system or even by airplanes. Thus also not directly neighboring nodes could be connected. Thereby the graph induces a network topology, which the discrete graph Laplacian strongly depends on.

Definition 2 (Laplacian matrix). Let G be a simple undirected graph with $N \in \mathbb{N}$ nodes. The Laplacian matrix¹ $L \in \mathbb{Z}^{N \times N}$ is defined as

$$L := A - D, \quad \text{i.e.,} \quad L_{ij} = \begin{cases} -\deg(v_i) & \text{if } i = j, \\ 1 & \text{if } i \neq j, \text{ and } v_i \text{ is adjacent to } v_j, \\ 0 & \text{otherwise,} \end{cases} \quad (5)$$

where $A \in \mathbb{N}^{N \times N}$ is the adjacency matrix of connections, $D \in \mathbb{N}^{N \times N}$ the degree matrix with number $\deg(v_i) = \sum_{j=1}^N A_{i,j}$ of connections from vertex v_i on the diagonal.

The Laplacian matrix on networks as simple undirected graphs is real valued, symmetric and negative semidefinite, i.e., its eigenvalues are real and nonpositive.

The equations for the SIR model on networks with node indices $i = 1, \dots, N$ are

$$\begin{aligned} \frac{dS_i}{dt} &= f(S_i, I_i) + d_{11} \sum_{j=1}^N L_{ij} S_j + d_{12} \sum_{j=1}^N L_{ij} I_j, \\ \frac{dI_i}{dt} &= g(S_i, I_i) + d_{22} \sum_{j=1}^N L_{ij} I_j, \\ \frac{dR_i}{dt} &= \gamma I - \delta R_i + d_{33} \sum_{j=1}^N L_{ij} R_j. \end{aligned} \quad (6)$$

In the following we only consider the equations for S and I , as the concentration R is not involved in the other two equations and can be separately determined by I . The natural zero-flux boundary conditions (4) for (2) are naturally incorporated in the adjacency and degree structure of the graph. If there is no diffusive connection from a node to another (external) node, there is no edge. Thus no external input or output is imposed.²

As network graphs we use two-dimensional lattices, where the nodes are equally arranged in a square lattice with distance 1. Only neighboring nodes within a Euclidean distance are connected. For distance 1 this results in the 5-point-stencil discretization of the Laplacian with degree 4 for interior nodes (LA4), for distance

¹In common graph literature this would be the negative Laplacian matrix.

²Technically graphs do not have boundaries. One way to create a Neumann boundary analogon would be an artificial layer of external nodes around Ω . As there is no flux along these edges they can be considered truncated and the degree reduced. Using a fixed geometrical realization of a lattice graph with artificial external nodes we can use, e.g., finite differences to yield the 5-point-stencil Laplace. For details see [3].

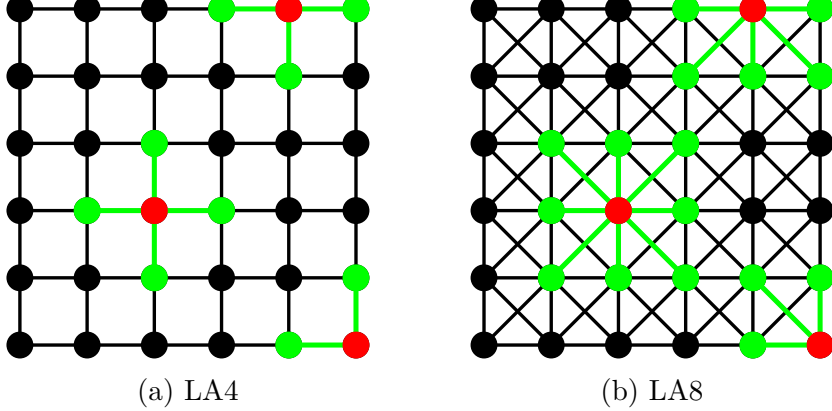


Figure 1: Network graphs with selected nodes (red) and associated neighbors (green), $N = 36$

$\sqrt{2}$ we get interior nodes with degree 8 (LA8), see Figure 1. In [2] further neighbor stencils and also random graphs like Erdős-Rényi and Barábasi-Albert are considered.

3 Steady states and linearization

To analyze the possibilities of diffusion-driven instabilities (DDI) we have to find stable homogeneous steady states $\bar{S} > 0$ and $\bar{I} > 0$ in absence of any diffusion, that are unstable if diffusion is active. Solving the reaction terms $f(\bar{S}, \bar{I}) \stackrel{!}{=} 0$ and $g(\bar{S}, \bar{I}) \stackrel{!}{=} 0$ provide three solutions, where $\theta := \delta + \mu + \gamma$,

$$\begin{aligned} (\bar{S}^{(1)}, \bar{I}^{(1)}) &= \left(\frac{\alpha}{\delta}, 0 \right), \\ (\bar{S}^{(2)}, \bar{I}^{(2)}) &= \left(\frac{\alpha}{2\delta} + \frac{\sqrt{\alpha^2\beta^2 - 4\beta\delta\theta^2}}{2\beta\delta}, \frac{\alpha}{2\theta} - \frac{\sqrt{\alpha^2\beta^2 - 4\beta\delta\theta^2}}{2\beta\theta} \right), \\ (\bar{S}^{(3)}, \bar{I}^{(3)}) &= \left(\frac{\alpha}{2\delta} - \frac{\sqrt{\alpha^2\beta^2 - 4\beta\delta\theta^2}}{2\beta\delta}, \frac{\alpha}{2\theta} + \frac{\sqrt{\alpha^2\beta^2 - 4\beta\delta\theta^2}}{2\beta\theta} \right). \end{aligned}$$

The first two states are no valid candidates for DDI as $(\bar{S}^{(1)}, \bar{I}^{(1)})$ is linearly stable, which is obvious as no infection can occur with no infectious individuals, and $(\bar{S}^{(2)}, \bar{I}^{(2)})$ is unstable. In the following we denote $\bar{S} := \bar{S}^{(3)}$ and $\bar{I} := \bar{I}^{(3)}$.

For perturbed concentrations

$$S_i(t) = \bar{S} + \tilde{S}(t), \quad I_i(t) = \bar{I} + \tilde{I}(t)$$

we use Hartman–Grobman linearizing theorem for the network system (2) around this equilibrium. It yields for every node $i = 1, \dots, N$

$$\begin{aligned} \frac{d\tilde{S}_i}{dt} &= \frac{\partial f}{\partial S}(\bar{S}, \bar{I})\tilde{S}_i + \frac{\partial f}{\partial I}(\bar{S}, \bar{I})\tilde{I}_i + d_{11} \sum_{j=1}^N L_{ij}\tilde{S}_j + d_{12} \sum_{j=1}^N L_{ij}\tilde{I}_j, \\ \frac{d\tilde{I}_i}{dt} &= \frac{\partial g}{\partial S}(\bar{S}, \bar{I})\tilde{S}_i + \frac{\partial g}{\partial I}(\bar{S}, \bar{I})\tilde{I}_i + d_{22} \sum_{j=1}^N L_{ij}\tilde{I}_j. \end{aligned} \quad (7)$$

4 Diffusion-driven instability

The remaining analysis uses the eigenvector basis of the symmetric, negative semidefinite network Laplacian. For eigenvalues λ_k , and associated eigenvectors $(\Phi_k = (\phi_1^{(k)}, \dots, \phi_N^{(k)})^T, k = 1, \dots, N)$, it holds

$$L\Phi_k = \lambda_k\Phi_k, \quad k = 1, \dots, N. \quad (8)$$

As an ansatz for the solution of differential equations for the perturbations we choose

$$\tilde{S}_i(t) = \sum_{k=1}^N c_k^S e^{\omega_k t} \phi_i^{(k)} \quad \text{and} \quad \tilde{I}_i(t) = \sum_{k=1}^N c_k^I e^{\omega_k t} \phi_i^{(k)}, \quad (9)$$

where the exponents ω_k can be interpreted as linear growth rates. Inserting in (7) and simplifying provides the eigenvalue problem

$$\omega_k \begin{pmatrix} c_k^S \\ c_k^I \end{pmatrix} = J(\lambda_k) \begin{pmatrix} c_k^S \\ c_k^I \end{pmatrix}, \quad \text{with } J(\lambda_k) := \begin{pmatrix} f_S + d_{11}\lambda_k & f_I + d_{12}\lambda_k \\ g_S & g_I + d_{22}\lambda_k \end{pmatrix}, \quad (10)$$

where f_S, f_I and g_S, g_I are the respective partial derivatives of the reaction terms evaluated at steady state (\bar{S}, \bar{I}) . We determine the growth rates ω_k by the trace and determinant formula for eigenvalues of 2×2 matrices

$$\omega_k = \frac{p(\lambda_k)}{2} \pm \frac{1}{4} \sqrt{p(\lambda_k)^2 - 4q(\lambda_k)}, \quad (11)$$

where $p(\lambda_k) := \text{Tr}(J(\lambda_k))$ and $q(\lambda_k) := \text{Det}(J(\lambda_k))$. As $(\bar{S}, \bar{I}) = (\bar{S}^{(3)}, \bar{I}^{(3)})$ is stable against perturbations for no diffusion, it holds $p(0) < 0$ and $q(0) > 0$. With all eigenvalues λ_k of L are nonpositive and the assumption of nonnegative self-diffusion parameters. This implies

$$p(\lambda_k) = f_S + g_I + (d_{11} + d_{22})\lambda_k < 0.$$

Thus only the growth rate with plus sign can become positive. We further denote this solution with ω_k .

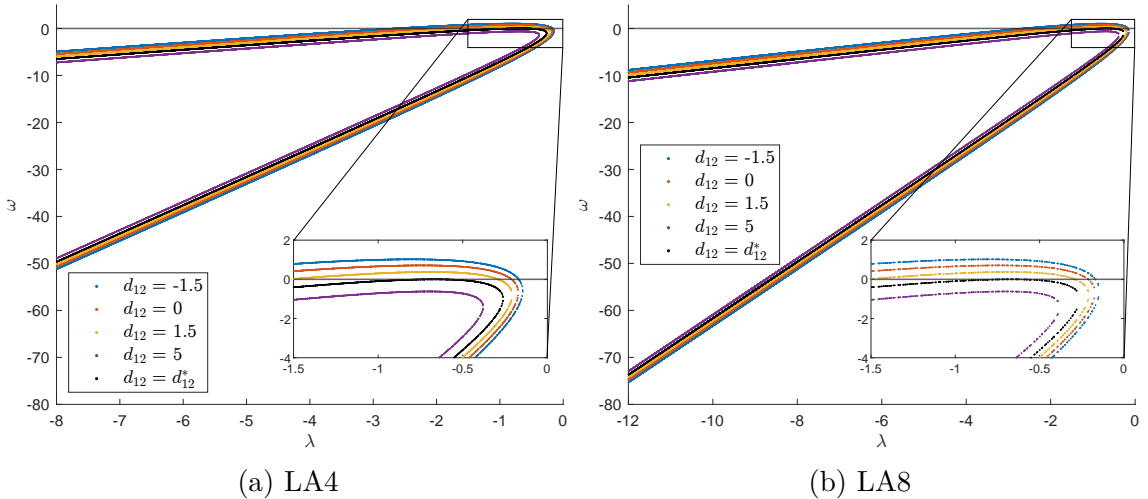


Figure 2: Growth rates ω for eigenvalues λ of network Laplacian matrix with $N = 10000$, different neighborhood stencils and cross-diffusion coefficients d_{12} , where critical cross-diffusion coefficient $d_{12}^* \approx 2.9968$.

For the emergence of diffusion-driven instabilities, i.e., Turing [4] patterns, we need the growth rate for at least one mode to be positive. We keep all parameters constant except the cross-diffusion coefficient d_{12} and determine the critical value d_{12}^* for which $\omega_k = 0$, that means $q(\lambda_k) = 0$. Geometrically interpreted this can be done by determining for which d_{12}^* the vertex of the parabola $q(\lambda_k)$ touches $q(\lambda_k) = 0$. For the spectrum of the Laplacian and the corresponding growth rates depending on the cross-diffusion coefficient see Figure 2.

Theorem 3 (Critical cross-diffusion coefficient for DDI). *Given the SIR network model (6) with cross-diffusion and zero-flux boundary conditions, diffusion-driven instabilities emerge if³ $d_{12} < d_{12}^*$, where*

$$d_{12}^* = \frac{1}{g_s} \left(f_S d_{22} + g_I d_{11} - 2\sqrt{d_{11} d_{22} (f_S g_I - f_I g_S)} \right). \quad (12)$$

Proof: Following the argumentation from above, we have to determine the minimum of $q(\lambda)$ by solving $\frac{\partial q}{\partial \lambda}(\lambda) \stackrel{!}{=} 0$ and inserting the solution into $q(\lambda) = 0$. This simple but lengthy calculation is omitted. \square

5 Numerical simulations

For the reproduction of the numerical results in [2], we choose the same parameters: $\alpha = 1$, $\beta = 35$, $\gamma = 1$, $\delta = 1$ and $\mu = 0.8$. For the self-diffusion coefficients we set $d_{11} = 6$ and $d_{22} = 1$. This results in an equilibrium state with $\bar{S} \approx 0.338755$ and $\bar{I} \approx 0.236159$ and a critical cross-diffusion coefficient $d_{12}^* \approx 2.996774733$. The initial condition is set as the approximate equilibrium state with added standard normal distributed noise of small magnitude

$$S_i(0) = \bar{S} + 10^{-5} \text{randn}(0, 1), \quad I_i(0) = \bar{I} + 10^{-5} \text{randn}(0, 1).$$

We simulated the model on a network with $N = 10000$ nodes, arranged in a square lattice of size 100×100 and use the neighborhood stencil LA4 for comparison with Chang et al. and LA8 for additional insights.

The model (6) seems practically a cellular automaton with von Neumann (LA4) and Moore (LA8) neighborhood if we discretize in time via Euler method. But to cope with the chosen diffusion coefficients and other parameters an explicit method is not applicable. To keep the code simple we use the ODE solver `ode15s` of `matlab`. The occurring memory problems for matrices with 20000×20000 entries are solved by setting the sparsity pattern of the Jacobian for `ode15s`.

By only changing the value for the cross-diffusion coefficient we get very different (beautiful) patterns. From red eye patterns in Figures 3a and 3b for negative cross-diffusion, i.e., diffusion of susceptibles to higher concentration of infectious, via

³In [2] Chang et al. derive $-d_{11}$ as lower bound, but that seems due to a typo in the definition of their $p(\mu_\nu)$ before.

snakes with red heads in Figure 3c for only self-diffusion. Positive cross-diffusion coefficients yield labyrinth patterns in Figure 3d that slowly change to mixed and finally only blue eye patterns in Figures 3e and 3f. For all these plots red denotes high concentrations of infectious individuals and blue denotes low concentrations.

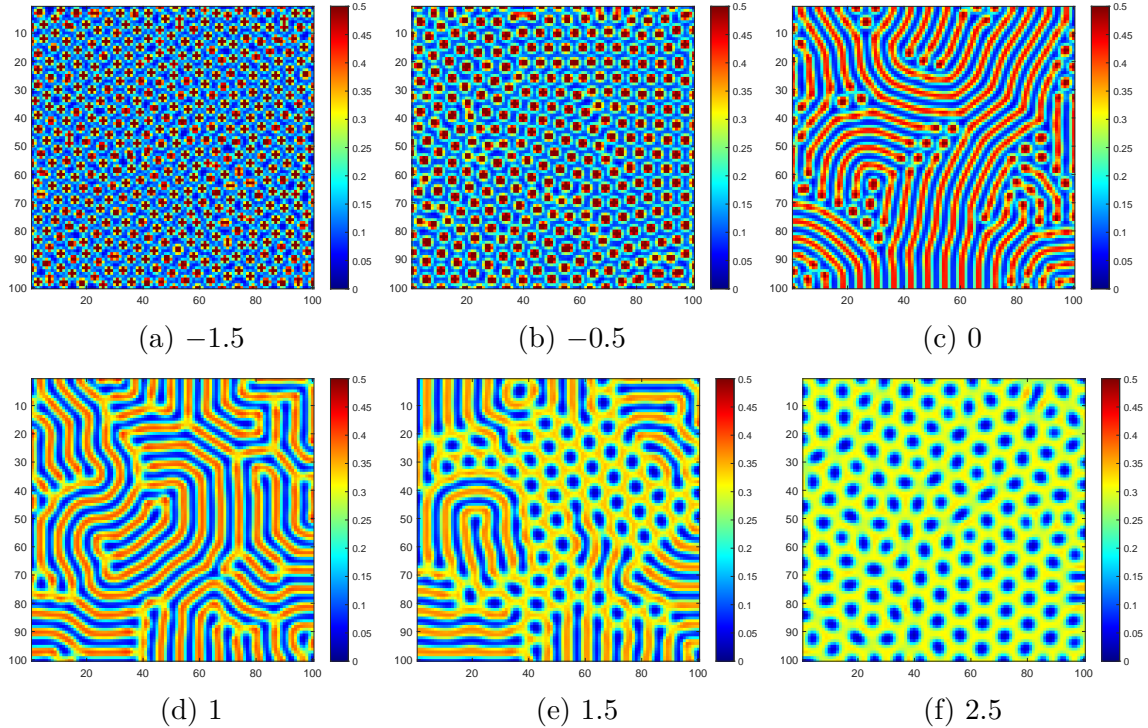


Figure 3: Turing patterns for concentration $I_i(1000)$ on lattice LA4 and different cross-diffusion coefficients d_{12}

For regular lattice networks with different neighbor stencils the structures in the emerging patterns are quite the same for different cross-diffusion coefficients. But the size of them scales with the degree of the nodes, which make sense, as the area of influence for diffusion grows, too. See Figure 4 or in [2]. For random networks, also see [2]. The effect of isolated spots for increasing d_{12} on nodes with high degree appears more clearly. This is remarkable and also makes sense from an infection related point of view as the density for groups with a high infection concentration decreases as d_{12} increases, while the group with lower concentrations is less affected. By simulations we can investigate the behavior around the critical value for cross-diffusion d_{12} , where for values greater but close enough to d_{12} oscillations appear. This is beyond the scope of this work, but will be presented⁴ in the Appendix.

⁴also see the videos on <https://github.com/loko58/ReactionDiffusionSIR>

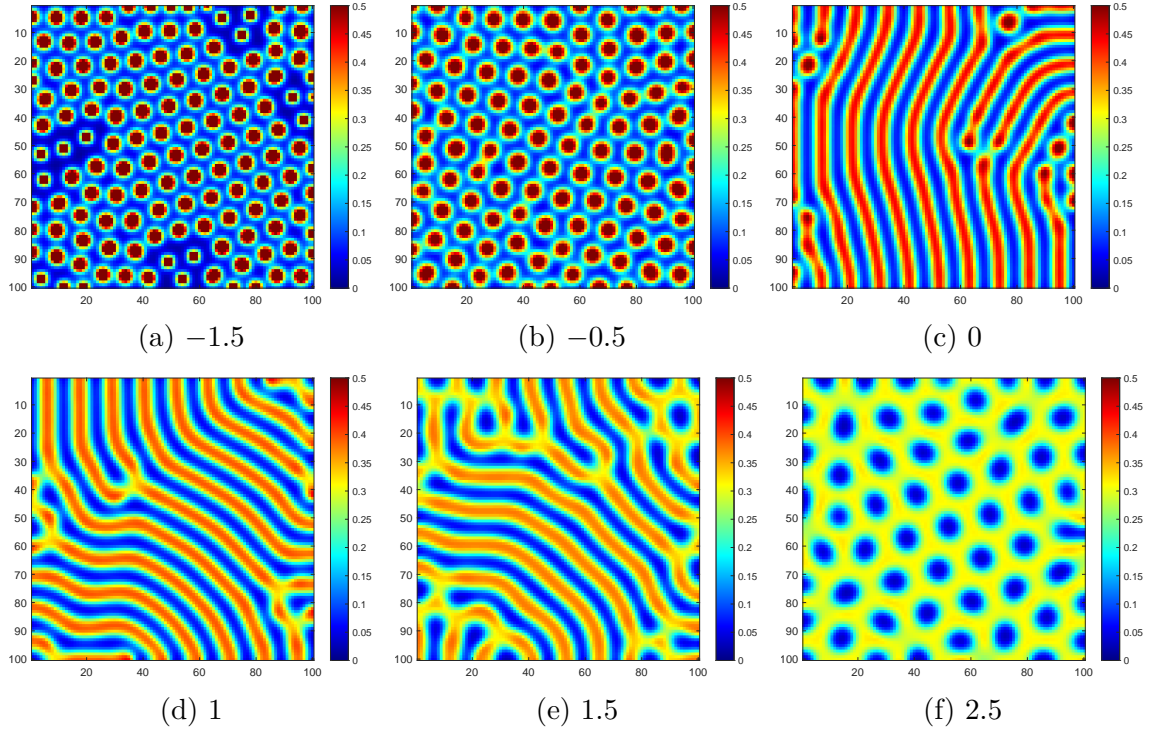


Figure 4: Turing patterns for concentration $I_i(1000)$ on lattice LA8 and different cross-diffusion coefficients d_{12}

References

- [1] W. O. Kermack, A. G. McKendrick, A Contribution to the Mathematical Theory of Epidemics. Proc. Roy. Soc. Lond. A 115, pp. 700-721, 1927.
- [2] L. Chang, M. Duan, G. Sun, Z. Jin, Cross-diffusion-induced patterns in an SIR epidemic model on complex networks. Chaos: An Interdisciplinary Journal of Nonlinear Science, 30(1), 013147, 2020.
- [3] L. Chang, C. Liu, G. Sun, Z. Wang, Z. Jin, Delay-induced patterns in a predator-prey model on complex networks with diffusion. New Journal of Physics, 21(7), 073035, 2019.
- [4] A. Turing, The Chemical Basis of Morphogenesis. Phil. Trans. R. Soc. Lond. B 237: pp. 37–72, 1952

A Appendix

To keep the main part of this report short but also to show some interesting effects, additional results are presented. *May they contribute to additional insights.*

At first we chose the same parameters as in [2]: $\alpha = 1$, $\beta = 35$, $\gamma = 1$, $\delta = 1$ and $\mu = 0.8$. For the self-diffusion coefficients we set $d_{11} = 6$ and $d_{22} = 1$. To check the influence of homogeneous versus heterogeneous initial values for LA4, we set the homogeneous initial condition as the equilibrium state with $\bar{S} \approx 0.338755$ and $\bar{I} \approx 0.236159$ and added for the heterogeneous a standard normal distributed (same seed for comparisons) noise of small magnitude (see Figure 5)

$$S_i(0) = \bar{S} + 10^{-5} \text{randn}(0, 1), \quad I_i(0) = \bar{I} + 10^{-5} \text{randn}(0, 1).$$

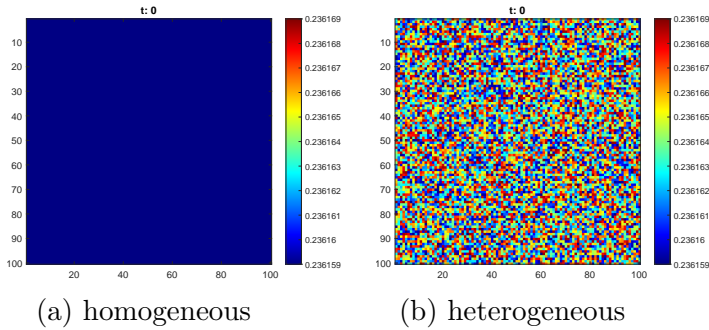


Figure 5: Different initial values for $I(0)$.

It seems that the pattern will still change a little bit even for $t > 1000$ (see Figure 7). We simulated values less than the critical cross-diffusion coefficient $d_{12}^* \approx 2.996774733$ and checked also one slightly greater (3) and one clearly greater (5) (see Figure 8 with flexible color bar). For $d_{12} = 3$ it seems like the pattern is fixed but oscillation by diffusion is added (see Figure 10 – Note the oscillatory behavior of error for $d_{12} = -1.5$, also!). The network had $N = 10000$ nodes, arranged in a square lattice of size 100×100 and use the neighborhood stencils LA4 and LA8. For convenience we only show the results for the concentration of infectious individuals.

Chang et al. chose big self-diffusion coefficients $d_{11} = 6$ and $d_{22} = 2$ to achieve a fast convergence towards a steady pattern. Therefore the basic patterns emerge quite suddenly - usually between $t = 10$ and $t = 50$ (see for $d_{12} \in \{-1.5, 0, 1.5\}$ in Figure 9). To highlight also the beautiful way of forming these patterns out of randomness we chose a flexible color bar.

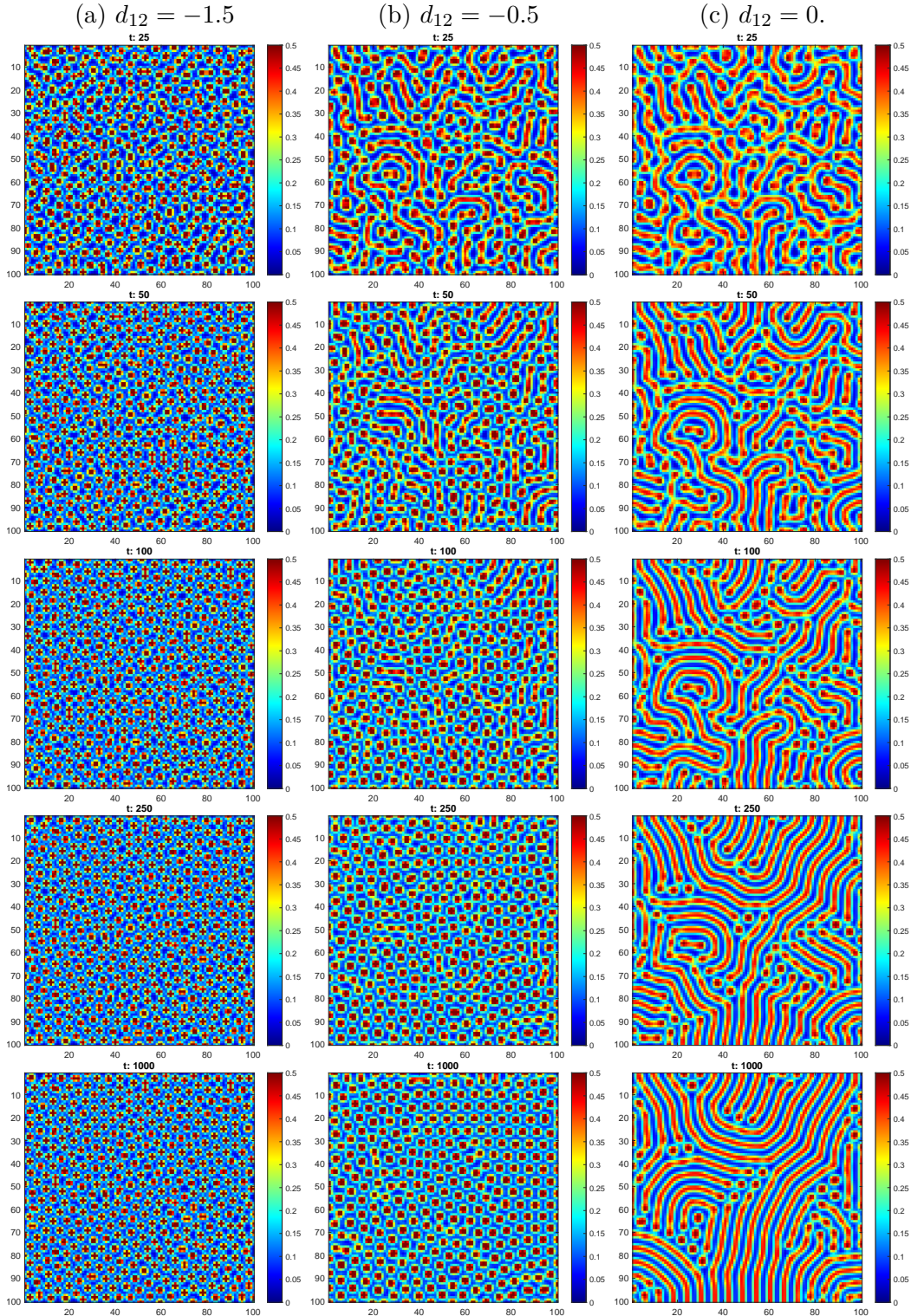


Figure 6: Emergence of Turing patterns for $t \in \{25, 50, 100, 250, 1000\}$ for LA4, different cross-diffusion coefficients d_{12} and initial values $S(0) = \bar{S}^{(3)} + 10^{-5}\text{randn}(0, 1)$, $I(0) = \bar{I}^{(3)} + 10^{-5}\text{randn}(0, 1)$.

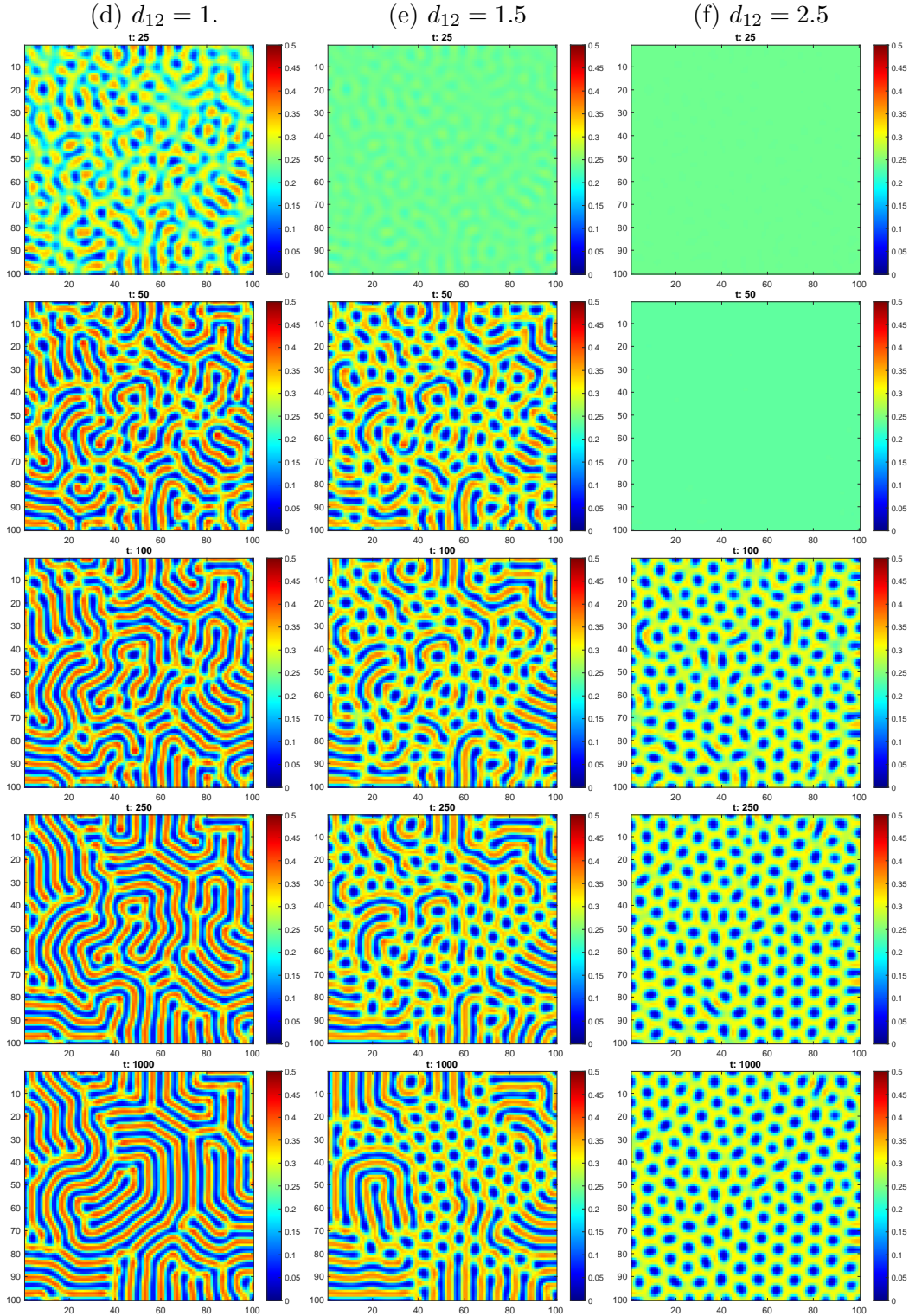


Figure 6: Emergence of Turing patterns for $t \in \{25, 50, 100, 250, 1000\}$ for LA4, different cross-diffusion coefficients d_{12} and initial values $S(0) = \bar{S}^{(3)} + 10^{-5}\text{randn}(0, 1)$, $I(0) = \bar{I}^{(3)} + 10^{-5}\text{randn}(0, 1)$.

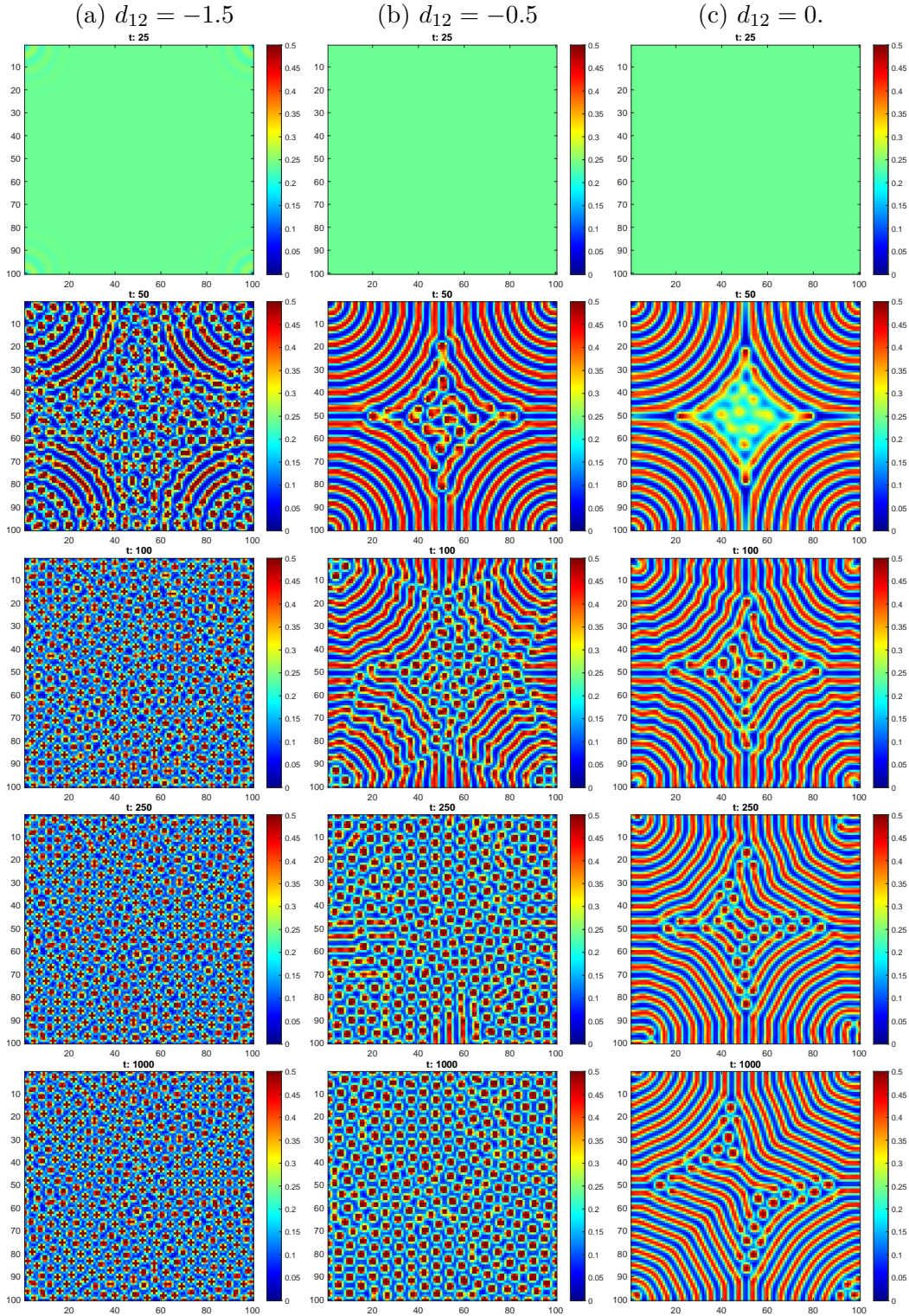


Figure 7: Emergence of Turing patterns for $t \in \{25, 50, 100, 250, 1000\}$ for LA4, different cross-diffusion coefficients d_{12} and initial values $S(0) = \bar{S}^{(3)}$, $I(0) = \bar{I}^{(3)}$.

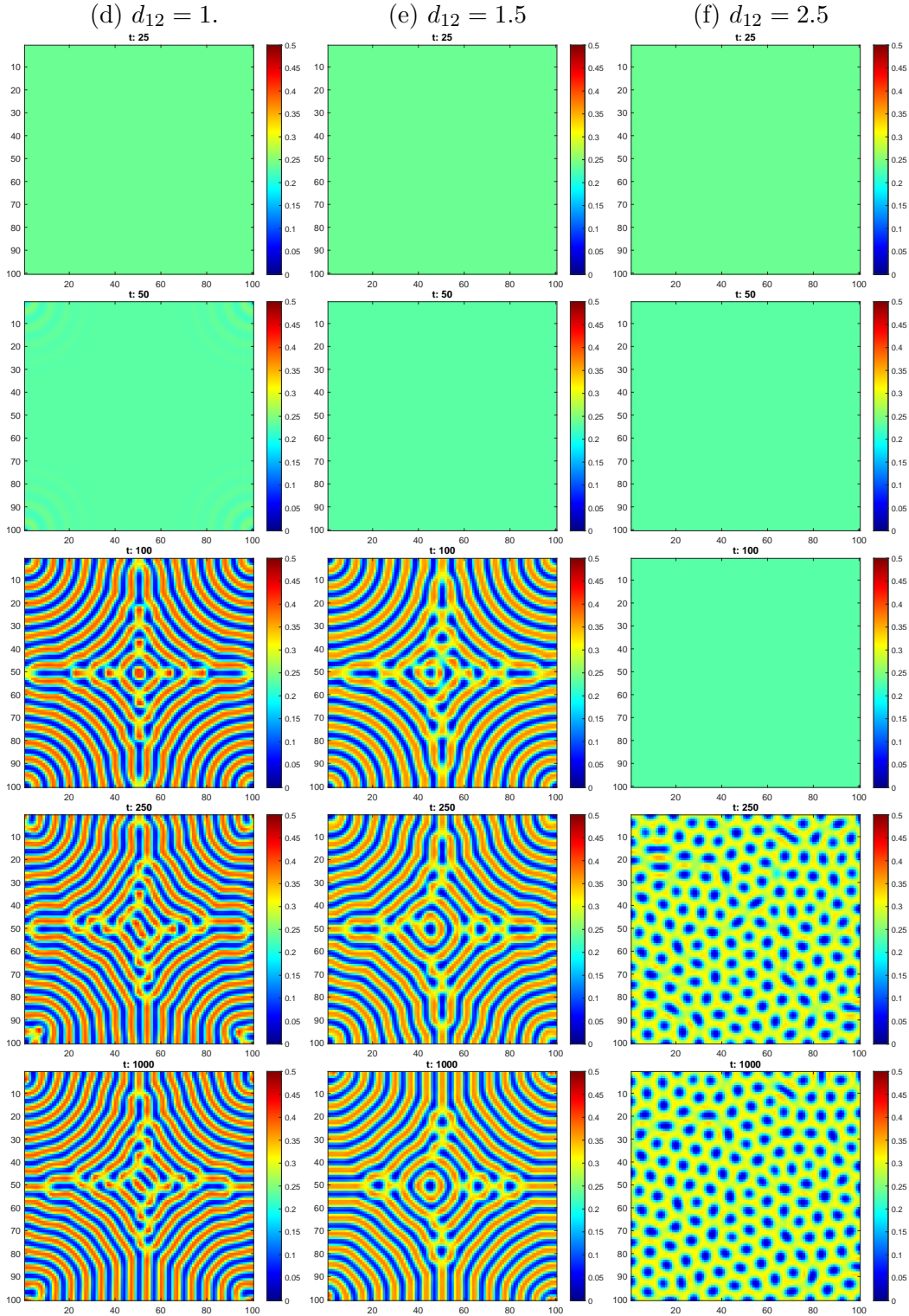


Figure 7: Emergence of Turing patterns for $t \in \{25, 50, 100, 250, 1000\}$ for LA4, different cross-diffusion coefficients d_{12} and initial values $S(0) = \bar{S}^{(3)}$, $I(0) = \bar{I}^{(3)}$.

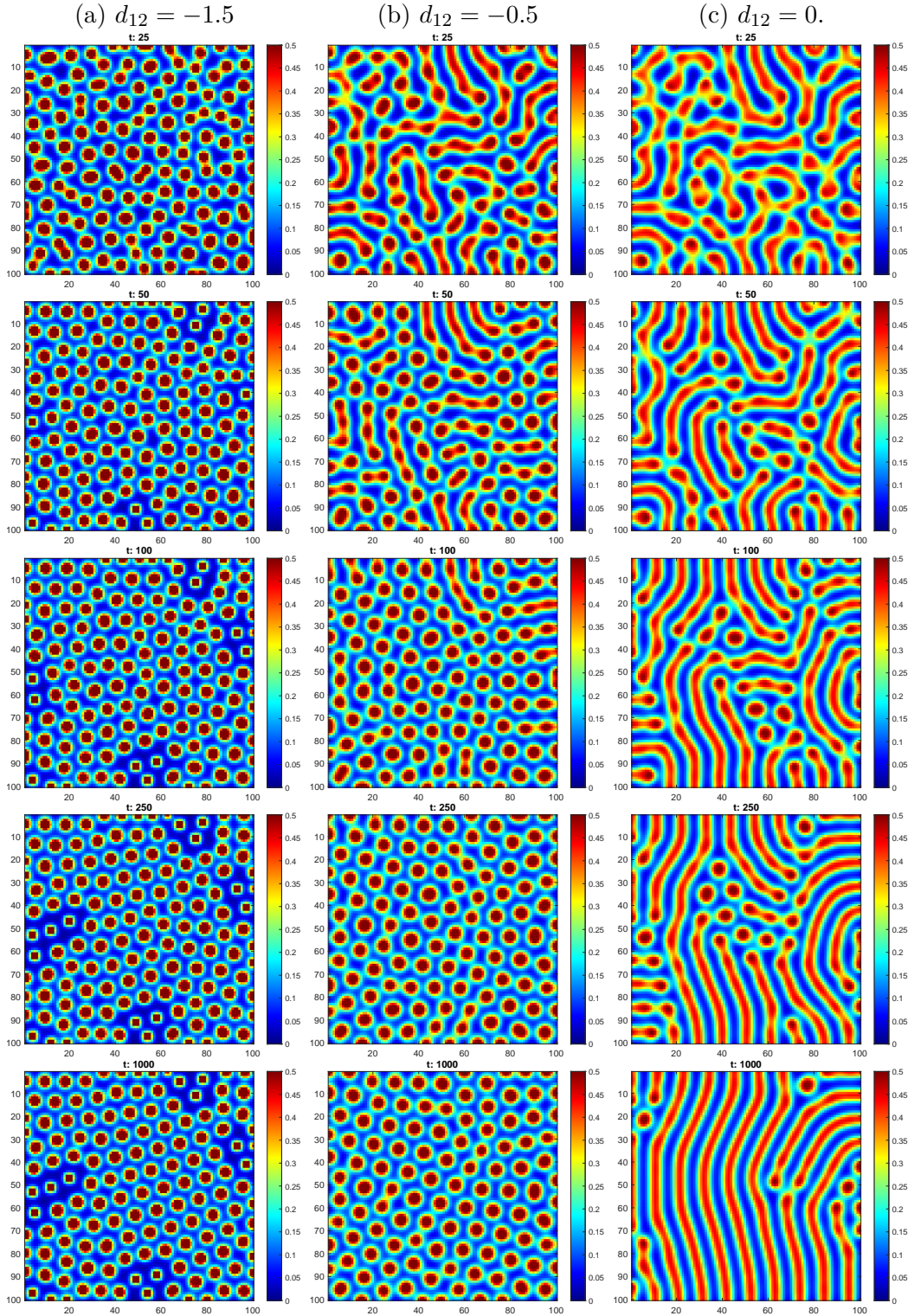


Figure 8: Emergence of Turing patterns for $t \in \{25, 50, 100, 250, 1000\}$ for LA8, different cross-diffusion coefficients d_{12} and initial values $S(0) = \bar{S}^{(3)} + 10^{-5}\text{randn}(0, 1)$, $I(0) = \bar{I}^{(3)} + 10^{-5}\text{randn}(0, 1)$.

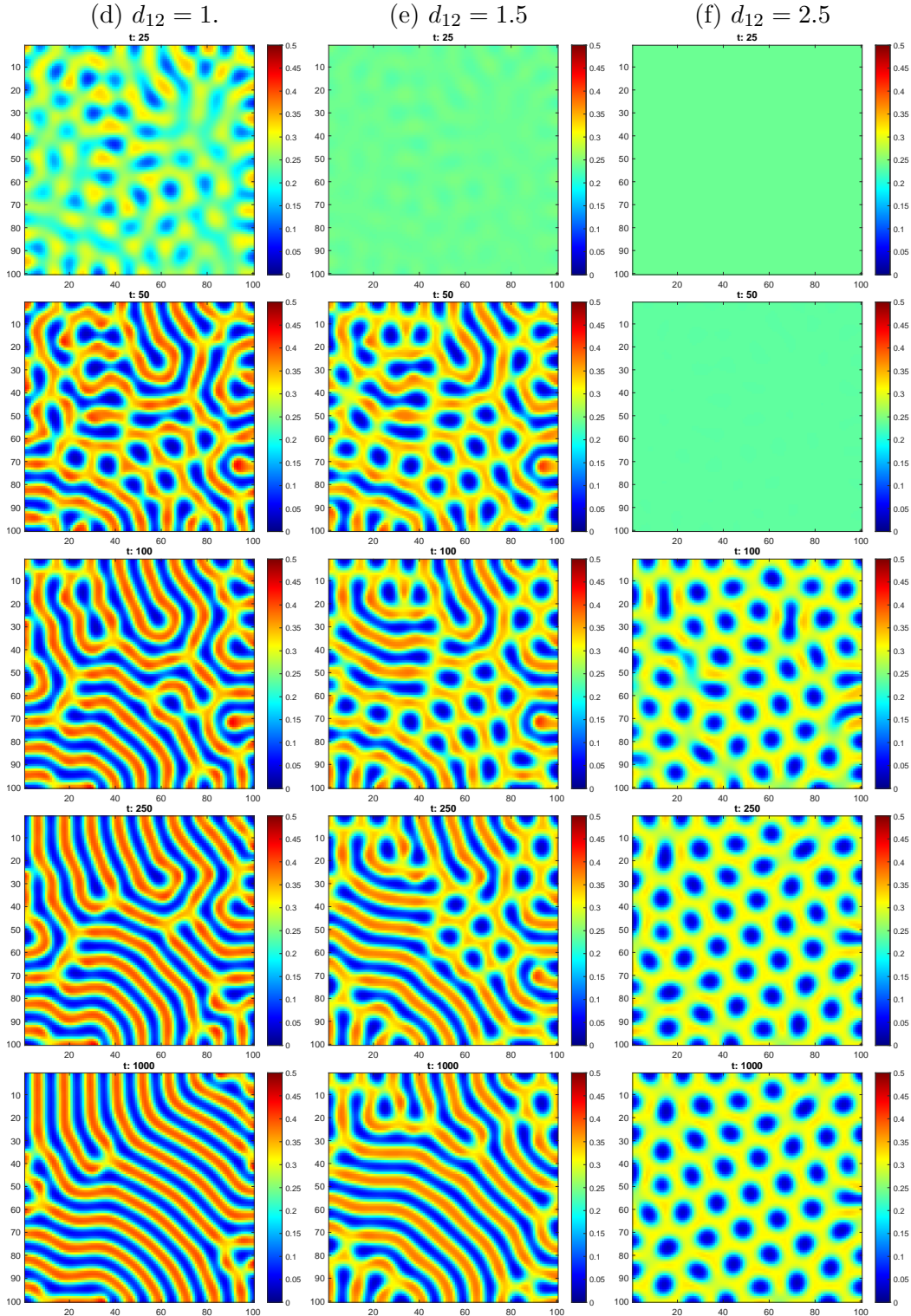


Figure 8: Emergence of Turing patterns for $t \in \{25, 50, 100, 250, 1000\}$ for LA8, different cross-diffusion coefficients d_{12} and initial values $S(0) = \bar{S}^{(3)} + 10^{-5}\text{randn}(0, 1)$, $I(0) = \bar{I}^{(3)} + 10^{-5}\text{randn}(0, 1)$.

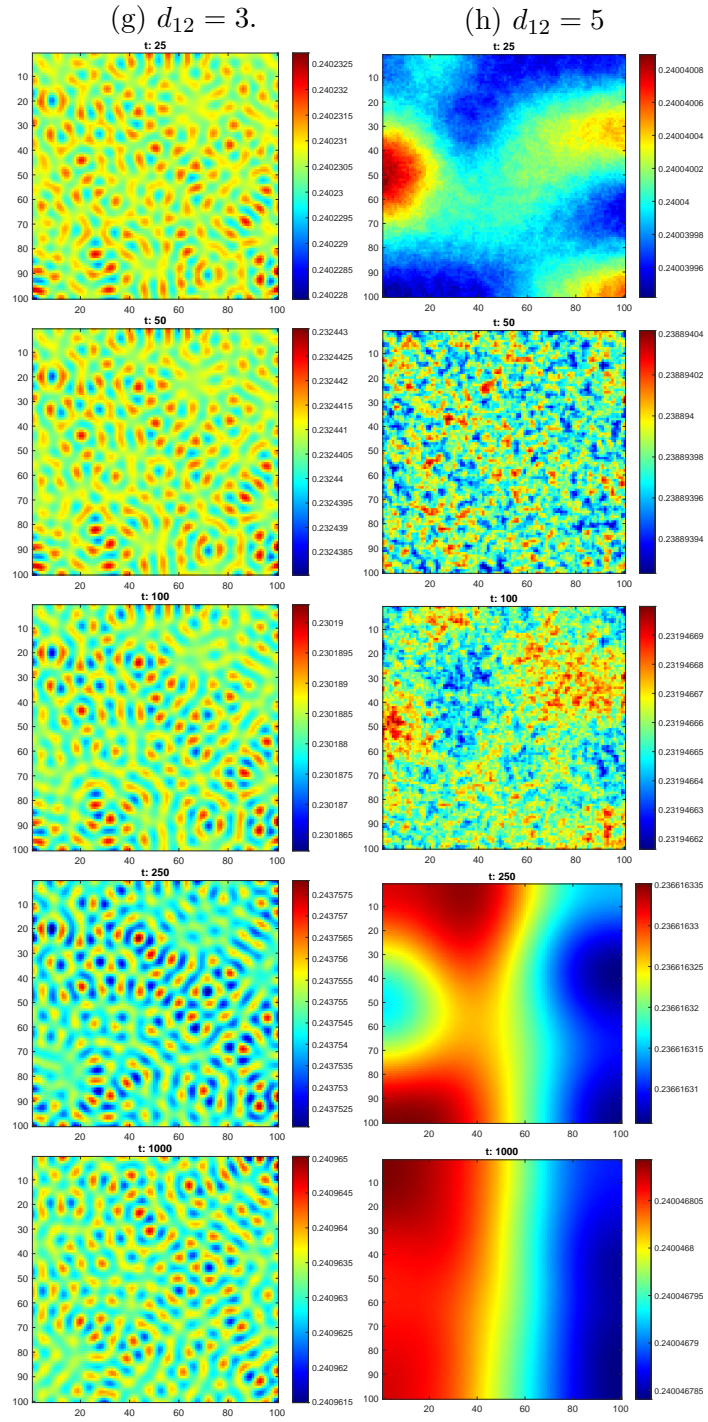


Figure 8: Emergence of Turing patterns for $t \in \{25, 50, 100, 250, 1000\}$ for LA4, different special cross-diffusion coefficients d_{12} and initial values $S(0) = \bar{S}^{(3)} + 10^{-5}\text{randn}(0, 1)$, $I(0) = \bar{I}^{(3)} + 10^{-5}\text{randn}(0, 1)$. Flexible color bar.

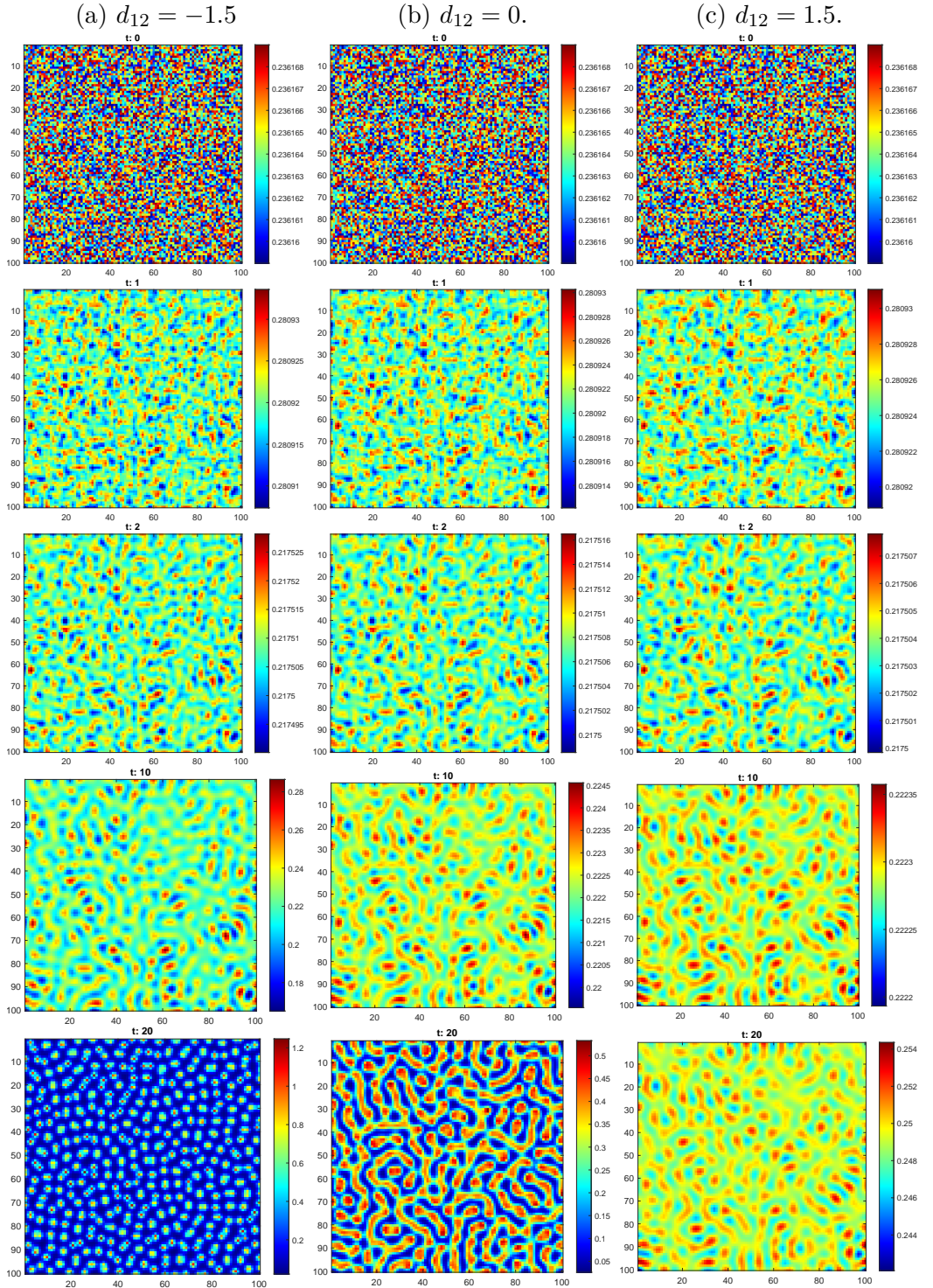


Figure 9: Beginning of Turing patterns for $t \in \{0, 1, 2, 10, 20\}$ for LA4, different cross-diffusion coefficients d_{12} and initial values $S(0) = \bar{S}^{(3)} + 10^{-5}\text{randn}(0, 1)$, $I(0) = \bar{I}^{(3)} + 10^{-5}\text{randn}(0, 1)$. Flexible color bar.

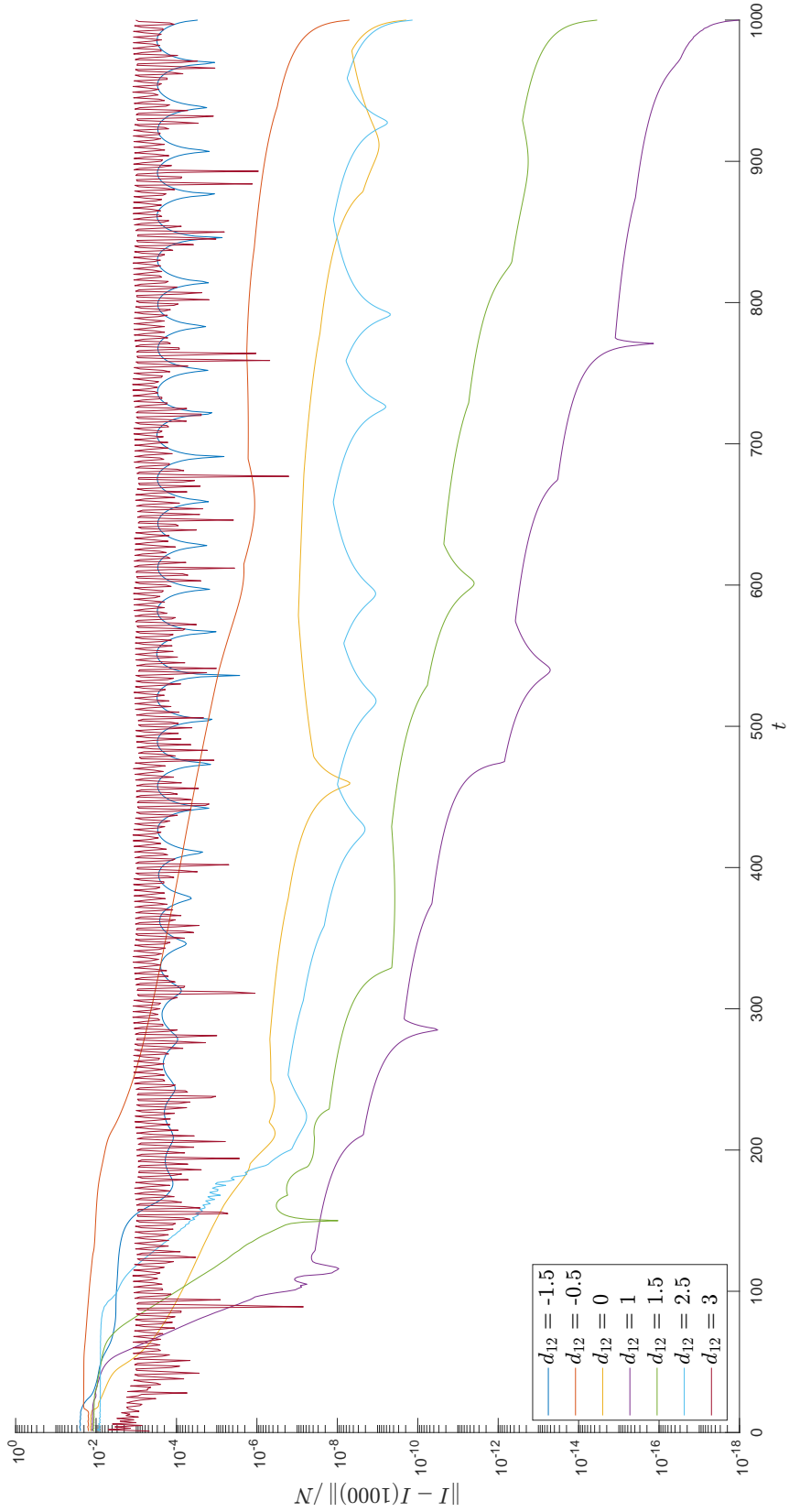


Figure 10: Convergence towards the patterns in the Euclidean norm $\|I - I(1000)\| / N$ with increasing time t . For L4, different cross-diffusion coefficients d_{12} and initial values $S(0) = \bar{S}^{(3)} + 10^{-5}\text{randn}(0, 1)$, $I(0) = \bar{I}^{(3)} + 10^{-5}\text{randn}(0, 1)$.